PHYSICAL REVIEW E **87**, 020104(R) (2013)

Everlasting initial memory threshold for rare events in equilibration processes

J. S. Lee,[1] Chulan Kwon,[2] and Hyunggyu Park[1]
[1]*School of Physics, Korea Institute for Advanced Study, Seoul 130-722, Korea*
[2]*Department of Physics, Myongji University, Yongin, Gyeonggi-Do 449-728, Korea*
(Received 26 September 2012; revised manuscript received 30 October 2012; published 13 February 2013)

Conventional wisdom indicates that initial memory should decay away exponentially in time for general (noncritial) equilibration processes. In particular, time-integrated quantities such as heat are presumed to lose initial memory in a sufficiently long-time limit. However, we show that the large deviation function of time-integrated quantities may exhibit initial memory effect even in the infinite-time limit, if the system is initially prepared sufficiently far away from equilibrium. For a Brownian particle dynamics, as an example, we found a sharp finite threshold rigorously, beyond which the corresponding large deviation function contains everlasting initial memory. The physical origin for this phenomenon is explored with an intuitive argument and also from a toy model analysis. Our results can be applied to general nonequilibrium relaxation processes reaching (non)equilibrium steady states.

DOI: 10.1103/PhysRevE.87.020104 PACS number(s): 05.70.Ln, 02.50.−r, 05.40.−a

Hot coffee gets colder and iced coffee gets warmer at room temperatures. These phenomena are the examples of equilibration processes and can be generalized as the following situation: a system with initial temperature T_s is in thermal contact with a heat bath with temperature T_b. Then, the system gradually deviates from its initial state and approaches the final equilibrium (EQ) state which is determined by the heat bath. Here, the initial distance from final equilibrium is parametrized by the temperature ratio $\beta \equiv T_b/T_s$. The relaxation process is usually exponentially fast, so the memory of the initial temperature will be lost for average values of most physical observables after a characteristic relaxation time. However, the initial memory can often survive in the tail part (rare-event region) of a probability distribution function (PDF) even in the long-time limit.

What about *time-integrated* quantities such as heat, work, or entropy production, which are the key quantities for nonequilibrium (NEQ) fluctuation theorems [1–5]? These accumulated quantities are also affected by a finite transient period, but their average values increase (or decrease) linearly in time asymptotically in NEQ steady state. Therefore, in a sufficiently long-time limit, our conventional wisdom may lead us to expect that they will lose all initial memory (independent of β). Nevertheless, in this Rapid Communication, we show rigorously that this is false wisdom for time-integrated quantities in the regime of rare events. Indeed, the tail of corresponding large deviation functions (LDF's) depends strongly on the initial condition (β) even in the infinite-time limit. On the other hand, the central region of the LDF's does not depend on β, and neither does the final steady state PDF, conforming to common sense. More surprisingly, there exists a sharp threshold for β^{-1} in general, only beyond which the initial memory lasts forever. This finite threshold are due to competition between the initial condition and the heat reservoir.

In the literature, there have been some reports that initial conditions can affect the large deviation function in the long-time limit [6–11]. For example, van Zon and Cohen [7] showed that heat transfer Q in a driven harmonic oscillator in contact with a heat bath violates the fluctuation theorem even in the long-time limit, starting initially from EQ [12]. This violation in the rare-event region has been measured quite accurately and confirmed by experiments in an equivalent electric-circuit setup [13]. In contrast to work, heat is known to satisfy the fluctuation theorem, only starting with a uniform distribution (infinite-temperature initial state) [14]. Thus, the violation of the fluctuation theorem can be interpreted as an example of everlasting initial memory effect in the large deviation function for heat.

In this Rapid Communication, we consider heat transfer during the equilibration process of a simple Brownian particle and investigate initial memory effects systematically in the long-time limit [15]. The Brownian particle dynamics is described by the Langevin equation

$$\dot{v} = -\gamma v + \xi, \tag{1}$$

where v is the velocity of the particle, γ is the dissipative coefficient, and ξ denotes a random white noise satisfying $\langle \xi(\tau)\xi(\tau')\rangle = 2D\delta(\tau - \tau')$. Here, we set the particle mass $m = 1$ for convenience and the heat bath temperature $T_b = D/\gamma$. Initially, the system is prepared in the EQ state with the Boltzmann distribution at temperature $T_s = T_b/\beta$. And then, the thermal contact is formed at time $\tau = 0$ between the system and the heat bath, and maintained until final time $\tau = t$.

Time-integrated heat flow between the system and the heat bath can be decomposed into the dissipated energy flow Q_d from the system into the heat bath and the injected energy flow Q_i in the other way around [6]:

$$Q_d \equiv \int_0^t d\tau \gamma v^2 \quad \text{and} \quad Q_i \equiv \int_0^t d\tau \xi v. \tag{2}$$

Even if the system reaches EQ in the long-time limit, each of $\langle Q_d\rangle$ and $\langle Q_i\rangle$ increases linearly in time t indefinitely with their difference representing the system energy change $\langle \Delta E\rangle = \frac{1}{2}[\langle v^2(t)\rangle - \langle v^2(0)\rangle]$, which is finite for nonzero β. As expected, there will be no net heat flow at EQ.

We first study the PDF of the (average) dissipated power, $\varepsilon_d \equiv Q_d/t$, and later the injected power, $\varepsilon_i \equiv Q_i/t$. To calculate the PDF, $P(\varepsilon_d)$, it is convenient to consider its

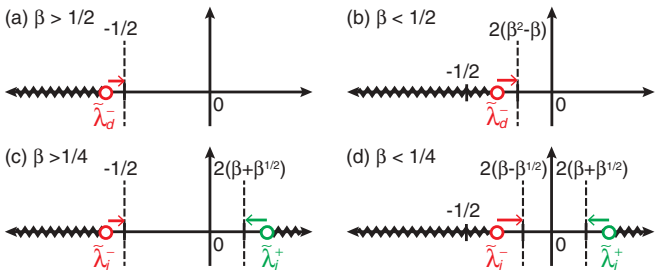

FIG. 1. (Color online) Panels (a) and (b) show the branch-cut structure of $\pi_d(\lambda)$ on the complex $\tilde{\lambda}$ plane for $\beta > 1/2$ and $\beta < 1/2$, respectively. Panels (c) and (d) show the branch-cut structure of $\pi_i(\lambda)$ for $\beta > 1/4$ and $\beta < 1/4$, respectively. Wiggled lines denote branch cuts. A head of an each arrow locates at its asymptotic value of the respective branch point as $t \to \infty$.

generating function,

$$\pi_d(\lambda) = \langle e^{-\lambda t \varepsilon_d} \rangle = \int_{-\infty}^{\infty} d\varepsilon_d P(\varepsilon_d) e^{-\lambda t \varepsilon_d}, \tag{3}$$

which is the Fourier transform of $P(\varepsilon_d)$. The generating function can be calculated exactly by the standard path integral method [6,16]. With the initial Boltzmann distribution $P_{\rm init}(v(0)) \sim \exp[-v^2(0)/(2T_s)]$ at temperature $T_s = D/(\gamma\beta)$, we find

$$\pi_d(\lambda) = e^{\gamma t/2} \left(\cosh \eta\gamma t + \frac{1+\tilde{\lambda}/\beta}{\eta} \sinh \eta\gamma t \right)^{-1/2}, \tag{4}$$

with dimensionless parameters $\tilde{\lambda} = 2D\lambda/\gamma$ and $\eta = \sqrt{1+2\tilde{\lambda}}$.

The inverse Fourier transform of Eq. (4) yields the PDF in terms of $\tilde{\varepsilon}_d \equiv \varepsilon_d/D$ as

$$\begin{aligned} P(\tilde{\varepsilon}_d) &= \frac{\gamma t}{4\pi i} \int_{-i\infty}^{i\infty} d\tilde{\lambda} \pi_d(\gamma\tilde{\lambda}/2D) \exp\left[\frac{\gamma t \tilde{\varepsilon}_d \tilde{\lambda}}{2} \right] \\ &= \frac{\gamma t}{4\pi i} \int_{-i\infty}^{i\infty} d\tilde{\lambda} \frac{\exp\left[\frac{\gamma t}{2} (\tilde{\varepsilon}_d \tilde{\lambda} + 1) \right]}{\sqrt{\cosh \eta\gamma t + \frac{1+\tilde{\lambda}/\beta}{\eta} \sinh \eta\gamma t}}. \end{aligned} \tag{5}$$

For large t, the above integration can be carried out by the saddle point approximation. However, care should be taken due to the presence of the branch cut. Here, we take the branch cut on the real-$\tilde{\lambda}$ axis where

$$f \equiv \cosh \eta\gamma t + \frac{1+\tilde{\lambda}/\beta}{\eta} \sinh \eta\gamma t \tag{6}$$

becomes negative; see Fig. 1.

We locate the branch points for large t, which depend on β. Note that η is real and positive for $\tilde{\lambda} > -\frac{1}{2}$, while η becomes pure imaginary for $\tilde{\lambda} < -\frac{1}{2}$. For $\beta > \frac{1}{2}$, $f > 0$ and we have no branch points for $\tilde{\lambda} > -\frac{1}{2}$. Instead, we find them in the region of $\tilde{\lambda} < -\frac{1}{2}$ and the largest one is denoted by $\tilde{\lambda}_d^- \simeq -\frac{1}{2} + O(t^{-2})$. In the $t \to \infty$ limit, the branch point $\tilde{\lambda}_d^- = -\frac{1}{2}$ has no β dependence. For $\beta < \frac{1}{2}$, in contrast, f can become negative for $\tilde{\lambda} > -\frac{1}{2}$ and we find the branch point approaching $\tilde{\lambda}_d^- = -2\beta(1-\beta)$ as $t \to \infty$. Locations of $\tilde{\lambda}_d^-$'s and branch cuts are shown in Figs. 1(a) and 1(b). It turns out that the branch-cut structure plays a crucial role in determining the everlasting initial memory effect.

From Eq. (5), one may easily expect for large t

$$P(\tilde{\varepsilon}_d) \simeq \exp[t h_t(\tilde{\varepsilon}_d)] \tag{7}$$

with the large deviation function (LDF) $h(\tilde{\varepsilon}_d) \equiv \lim_{t\to\infty} h_t(\tilde{\varepsilon}_d)$. We first calculate the LDF using the saddle point method in the presence of the branch-cut structure found as above. For large t, Eq. (6) becomes $f \simeq \frac{1}{2} e^{\eta\gamma t}(1 + \frac{1+\tilde{\lambda}/\beta}{\eta})$. The saddle point $\tilde{\lambda}_d^*$ is given by the solution of the following equation:

$$\frac{d}{d\tilde{\lambda}} \left[\frac{\gamma t}{2} (\tilde{\varepsilon}_d \tilde{\lambda} + 1 - \eta) - \frac{1}{2} \ln \left(1 + \frac{1+\tilde{\lambda}/\beta}{\eta} \right) \right] = 0, \tag{8}$$

where the logarithmic term is included because it may become very large in the vicinity of $\tilde{\lambda} = -2\beta(1-\beta)$ for $\beta < \frac{1}{2}$.

For $\beta > \frac{1}{2}$, we find a solution (saddle point) on the real-$\tilde{\lambda}$ axis which is outside of the branch cut as

$$\tilde{\lambda}_d^* = -\frac{1}{2} \left(1 - \frac{1}{\tilde{\varepsilon}_d^2} \right), \tag{9}$$

as $t \to \infty$. Then, the LDF for $\beta > 1/2$ becomes

$$h(\tilde{\varepsilon}_d) = \frac{\gamma}{2} (\tilde{\varepsilon}_d \tilde{\lambda}_d^* + 1 - \eta^*) = -\frac{\gamma}{4\tilde{\varepsilon}_d} (\tilde{\varepsilon}_d - 1)^2, \tag{10}$$

where $\eta^* = \sqrt{1+2\tilde{\lambda}_d^*}$ and the logarithmic term is negligible. As $P(\tilde{\varepsilon}_d) = 0$ for $\tilde{\varepsilon}_d \leqslant 0$, the LDF is defined only for $\tilde{\varepsilon}_d > 0$. This LDF has no β dependence but is determined only by the heat bath properties (γ, D). Thus, we call Eq. (10) the heat-bath characteristic curve (HBCC).

For $\beta < \frac{1}{2}$, the saddle point location exhibits a nonanalytic behavior as a function of $\tilde{\varepsilon}_d$, due to the interplay of the saddle point and the branch point. When $\tilde{\varepsilon}_d < (1-2\beta)^{-1}$, the saddle point $\tilde{\lambda}_d^*$ given by Eq. (9) is located to the right of the branch point, $\tilde{\lambda}_d^* > \tilde{\lambda}_d^- = -2\beta(1-\beta)$, in the $t \to \infty$ limit. Thus, the LDF $h(\tilde{\varepsilon}_d)$ is identical to the HBCC in Eq. (10). When $\tilde{\varepsilon}_d > (1-2\beta)^{-1}$, the saddle point approaches the branch point asymptotically from the right side, due to the divergence of the logarithmic term in Eq. (8) at the branch point. However, as this approach is not exponentially fast in time, the dominant contribution to the LDF comes from the conventional first term in Eq. (8) at the asymptotic saddle point $\tilde{\lambda}_d^* = \tilde{\lambda}_d^- = -2\beta(1-\beta)$. Summarizing for $\beta < \frac{1}{2}$, the LDF is

$$h(\tilde{\varepsilon}_d) = \begin{cases} -\frac{\gamma}{4\tilde{\varepsilon}_d} (\tilde{\varepsilon}_d - 1)^2, & \tilde{\varepsilon}_d < \frac{1}{1-2\beta}, \\ -\gamma\beta[(1-\beta)\tilde{\varepsilon}_d - 1], & \tilde{\varepsilon}_d > \frac{1}{1-2\beta}. \end{cases} \tag{11}$$

Note that the LDF for large $\tilde{\varepsilon}_d$ is deformed from the HBCC and has the initial condition (β) dependence; see Figs. 2(a) and 2(b).

Our results show that, for sufficiently high initial temperatures ($\beta < \frac{1}{2}$), the initial memory survives forever in the large $\tilde{\varepsilon}_d$ region of the LDF and completely vanishes below the threshold of the initial temperature ($\beta > \frac{1}{2}$). Large dissipated energy Q_d is generated by the decay of highly energetic particles with energy $\sim Q_d$. There are two distinct sources for highly energetic particles; (a) heat bath and (b) initial Boltzmann distribution, which compete with each other. We estimate the probability P_a and P_b to find a particle to

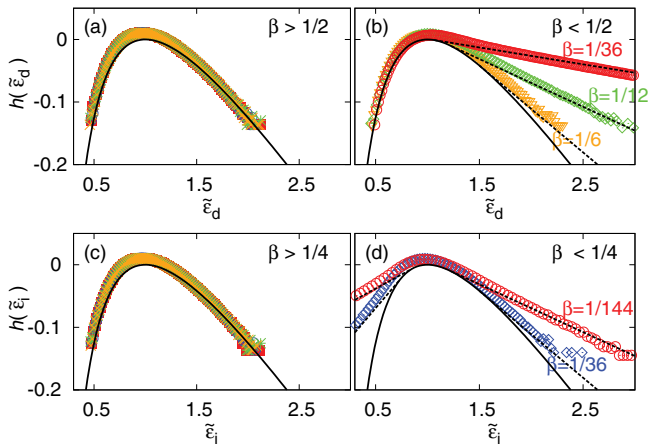

FIG. 2. (Color online) Panels (a) and (b) are the LDF's of the dissipated power for $\beta > 1/2$ and $\beta < 1/2$, respectively. The solid line is the HBCC [see Eq. (10)]. In (a) $\times$, $*$, $\circ$, and $\blacksquare$ are numerical data for $\beta = 3/4$, 1, 2, and 4, respectively. Panels (c) and (d) are the LDF's of the injected power for $\beta > 1/4$ and $\beta < 1/4$, respectively. In (c) $\times$, $*$, $\circ$, and $\blacksquare$ are numerical data for $\beta = 1/2$, 1, 2, and 4, respectively. Each dashed line denotes the analytic line for each β. All numerical results are obtained at $t = 100$.

dissipate energy Q_d from each source, respectively. From the HBCC in Eqs. (7) and (10), we find $P_a \sim \exp[-Q_d/(4T_b)]$ for large $\widetilde{\varepsilon}_d$. On the other hand, we assume that a particle with high initial energy decays by the deterministic dynamics of $\dot{v} = -\gamma v$. In this case, the dissipated energy is $Q_d = \frac{1}{2}v^2(0)$ in the long-time limit. Thus, we estimate $P_b \sim \exp[-Q_d/T_s] = \exp[-\beta Q_d/T_b]$ from the initial Boltzmann distribution at temperature T_s. As a result, the HBCC P_a dominates over P_b for $\beta > \frac{1}{4}$ or the initial memory dominates, otherwise. As Q_d is overestimated in the latter case, the threshold value $\frac{1}{4}$ only sets its lower bound, which is consistent with the correct value $\beta_d^c = \frac{1}{2}$.

We also calculate the leading finite-time correction of $h_t(\widetilde{\varepsilon}_d)$ in Eq. (7). As the leading correction is $O(\ln t/t)$, it yields a power-law type prefactor to the exponential form of the PDF, $P(\widetilde{\varepsilon}_d)$. For $\beta < \frac{1}{2}$, it is tricky to calculate this correction because the saddle point is very close to the branch point. In fact, it cannot be obtained through a conventional Gaussian integral. Here, we just report our result without presenting details [17] for $\beta < \frac{1}{2}$,

$$P(\widetilde{\varepsilon}_d) = \begin{cases} \frac{\sqrt{\gamma t}c_d(\beta)}{\widetilde{\varepsilon}_d\sqrt{(\widetilde{\varepsilon}_d+1)[(2\beta-1)\widetilde{\varepsilon}_d+1]}} e^{-(\gamma t/4\widetilde{\varepsilon}_d)(\widetilde{\varepsilon}_d-1)^2} & \text{(A)}, \\ (\gamma t)^{3/4} r(\beta) e^{-\gamma\beta t[(1-\beta)\widetilde{\varepsilon}_d-1]} & \text{(B)}, \\ \frac{\sqrt{\gamma t}s(\beta)}{\sqrt{\widetilde{\varepsilon}_d-1/(1-2\beta)}} e^{-\gamma\beta t[(1-\beta)\widetilde{\varepsilon}_d-1]} & \text{(C)}, \end{cases} \quad (12)$$

where there are three regions: (A) $(1-2\beta)^{-1} - \widetilde{\varepsilon}_d \gg (\gamma t)^{-1/2}$; (B) $|\widetilde{\varepsilon}_d - (1-2\beta)^{-1}| \ll (\gamma t)^{-1/2}$; (C) $\widetilde{\varepsilon}_d - (1-2\beta)^{-1} \gg (\gamma t)^{-1/2}$. Three constants are given as $c_d(\beta) = \sqrt{\beta/\pi}$, $r(\beta) = \sqrt{2\beta}(1-2\beta)^{7/4}\Gamma(\frac{1}{4})/(4\pi\sqrt{1-\beta})$, and $s(\beta) = \sqrt{\beta}(1-2\beta)/\sqrt{\pi(1-\beta)}$. For $\beta > \frac{1}{2}$, the PDF is given by the same one in (A) of Eq. (12) for all $\widetilde{\varepsilon}_d > 0$. The prefactors depend on the initial condition (β) for all cases, as expected, but their power-law exponent in terms of $\widetilde{\varepsilon}_d$ changes abruptly from -2 to $-\frac{1}{2}$ as $\widetilde{\varepsilon}_d$ increases. It is interesting to note that this exponent change is very similar to what was found dynamically for the PDF of nonequilibrium work in simple linear diffusion systems [18].

Now, we turn to the injected power, $\varepsilon_i = Q_i/t$. The calculation method is almost the same as before. We obtain the generating function of the injected power as

$$\pi_i(\lambda) = e^{\gamma t/2}\left(\cosh\eta\gamma t + \frac{1+\widetilde{\lambda}-\widetilde{\lambda}^2/2\beta}{\eta}\sinh\eta\gamma t\right)^{-1/2}. \quad (13)$$

Compared to Eq. (4), there is only a parametric difference in the coefficient of the hyperbolic sine term. We can obtain the PDF of the dimensionless injected power, $P(\widetilde{\varepsilon}_i)$ with $\widetilde{\varepsilon}_i \equiv \varepsilon_i/D$, by performing the inverse Fourier transform of $\pi_i(\lambda)$.

Similar to the case of the dissipated power, the branch points are determined by the equation

$$0 = \cosh\eta\gamma t + \frac{1+\widetilde{\lambda}-\widetilde{\lambda}^2/2\beta}{\eta}\sinh\eta\gamma t. \quad (14)$$

We find two relevant solutions of Eq. (14); one is on the positive real axis, $\widetilde{\lambda}_i^+$, and the other is on the negative real axis, $\widetilde{\lambda}_i^-$, as shown in Figs. 1(c) and 1(d), respectively. In the $t \to \infty$ limit, one can show that $\widetilde{\lambda}_i^+ = 2(\beta + \sqrt{\beta})$ for all β, while $\widetilde{\lambda}_i^- = -\frac{1}{2}$ for $\beta > \frac{1}{4}$ and $\widetilde{\lambda}_i^- = -2(\sqrt{\beta} - \beta)$ for $\beta < \frac{1}{4}$.

By defining the LDF, $h(\widetilde{\varepsilon}_i)$, for $\widetilde{\varepsilon}_i$ in the $t \to \infty$ limit and through a similar algebra, we find for $\beta > \frac{1}{4}$

$$h(\widetilde{\varepsilon}_i) = \begin{cases} -\gamma\sqrt{\beta}[1-(1+\sqrt{\beta})\widetilde{\varepsilon}_i], & \widetilde{\varepsilon}_i < \frac{1}{1+2\sqrt{\beta}}, \\ -\frac{\gamma}{4\widetilde{\varepsilon}_i}(\widetilde{\varepsilon}_i - 1)^2, & \widetilde{\varepsilon}_i > \frac{1}{1+2\sqrt{\beta}}. \end{cases} \quad (15)$$

For $\beta < \frac{1}{4}$, the LDF becomes

$$h(\widetilde{\varepsilon}_i) = \begin{cases} -\gamma\sqrt{\beta}[1-(1+\sqrt{\beta})\widetilde{\varepsilon}_i], & \widetilde{\varepsilon}_i < \frac{1}{1+2\sqrt{\beta}}, \\ -\frac{\gamma}{4\widetilde{\varepsilon}_i}(\widetilde{\varepsilon}_i - 1)^2, & \frac{1}{1+2\sqrt{\beta}} < \widetilde{\varepsilon}_i < \frac{1}{1-2\sqrt{\beta}}, \\ -\gamma\sqrt{\beta}[(1-\sqrt{\beta})\widetilde{\varepsilon}_i - 1], & \widetilde{\varepsilon}_i > \frac{1}{1-2\sqrt{\beta}}. \end{cases} \quad (16)$$

Our results read that the negative tail always displays the singularity ($\widetilde{\lambda}_i^+$), including the $\beta = 1$ case. This indicates that the nonanalytic branch in the negative tail has nothing to do with the equilibration (relaxation) process, but comes from a rather trivial constraint: The energy loss of a particle is bounded by its initial energy E_0, so low-energy particles with initial energy $E_0 < |Q_i|$ could not contribute to the negative tail of the LDF. The probability to find high-energy particles with $E_0 > |Q_i|$ is roughly $\sim\exp[-\frac{\gamma\beta}{D}|Q_i|]$, which is consistent with the negative tail in Eqs. (15) and (16) for large β. However, the positive tail shows the threshold at $\beta_i^c = \frac{1}{4}$ where the high-energy particles originating from the initial condition start to dominate over those from the heat reservoir. Note that the threshold value varies with the quantity interested. The leading finite-time correction is rather complicated, which will appear elsewhere [17].

To confirm our analytic calculations in Eqs. (10), (11), (15), and (16), we performed numerical integrations of the Langevin equation, Eq. (1). Here, we set $\gamma = D = 1$, and integration time interval $\Delta t = 10^{-3}$. Figure 2(a) displays numerical data for $h(\widetilde{\varepsilon}_d)$ at $t = 100$ for various values of $\beta > 1/2$. Regardless of β, all numerical results collapse well onto the HBCC as expected from Eq. (10). Slight deviation from the analytic

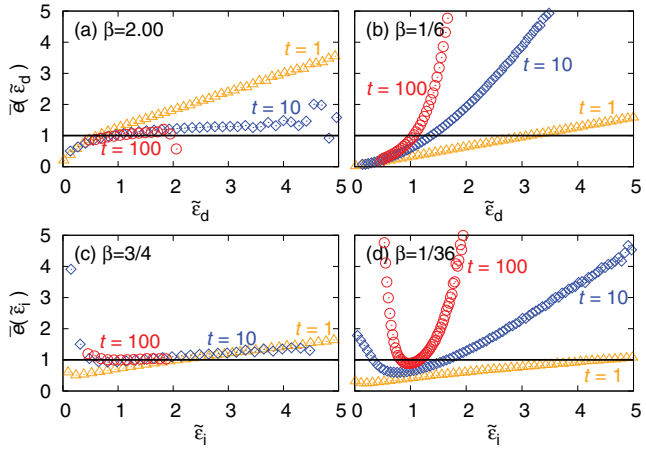

FIG. 3. (Color online) Panels (a) and (b) show the correlation in time between the initial energy and the dissipated power for $\beta > 1/2$ and $\beta < 1/2$, respectively. Panels (c) and (d) show the correlation between the initial energy and the injected power at time τ for $\beta > 1/4$ and $\beta < 1/4$, respectively. △, ◇, and ○ are data for $\tau = 1$, 10, and 100, respectively.

HBCC comes from the finite-time effect. We confirmed that the LDF with leading finite-time correction [see Eq. (12)] perfectly agrees with the numerical data at $t = 100$ (not shown here). Figure 2(b) shows $h(\widetilde{\varepsilon}_d)$ for $\beta < 1/2$. Numerical results also agree well with our analytic results in Eq. (11). Figures 2(c) and 2(d) show the LDF of the injected power for $\beta > 1/4$ and $\beta < 1/4$, respectively. In Fig. 2(c) the LDF for $\widetilde{\varepsilon}_i < (1 + 2\sqrt{\beta})^{-1}$ does not appear simply because the region is outside of the plot range. Meanwhile, the three regions are clearly seen in Fig. 2(d), as expected from Eq. (16).

To understand better the origin of the threshold β^c dividing different phases, we introduce a simple toy model. In order to examine the correlation between the initial energy and the average power, we define a function $\overline{E}_t(\widetilde{\varepsilon})$ which is the average initial energy of a particle whose average (dissipated or injected) power until time t is given by $\widetilde{\varepsilon}$. It is convenient to use the normalized function $\overline{e}(\widetilde{\varepsilon}) \equiv \overline{E}(\widetilde{\varepsilon})/\langle E\rangle_0$, with $\langle E\rangle_0$ the average initial energy without any constraint on its power. In Fig. 3(a), $\overline{e}(\widetilde{\varepsilon}_d)$ approaches the constant 1 for large t, which implies no correlation between the initial energy and the corresponding dissipation power. Thus, there will be no initial condition dependence on the PDF for large $\widetilde{\varepsilon}_d$. In contrast, Fig. 3(b) shows divergence of $\overline{e}(\widetilde{\varepsilon}_d)$ in time, which indicates that high initial energy is responsible for large $\widetilde{\varepsilon}_d$. Thus, the tail of the PDF, $P(\widetilde{\varepsilon}_d)$, should be dominated by a particle with high initial energy which is generated by the initial high-temperature distribution. This causes the deviation of $h(\widetilde{\varepsilon}_d)$ from the HBCC for $\widetilde{\varepsilon}_d > (1 - 2\beta)^{-1}$ when $\beta < \frac{1}{2}$ (higher initial temperatures). Figure 3(c) shows that $\overline{e}(\widetilde{\varepsilon}_i)$ approaches 1 for $\beta > 1/4$, while Fig. 3(d) shows its divergence for $\beta < 1/4$.

In summary, we consider the equilibration process of a Brownian particle system, starting from various initial temperatures different from the heat bath temperature. We calculate the LDF of time-integrated quantities like the dissipated energy and the injected energy due to the heat bath. Remarkably, we find a finite threshold for the initial temperature, only beyond which the positive LDF tail contains everlasting initial memory. We argue that this is due to the competition of highly energetic particles originating from the heat bath and from the initial distribution. In contrast, the negative LDF tail of the injected energy or total heat always displays the nonanalytic branches due to the trivial constraint.

Our simple toy model analysis supports this argument by showing that large dissipated energy is generated dominantly by particles with high initial energy, rather than by highly energetic particles randomly generated by the heat bath, when the initial temperature is sufficiently high enough with respect to the heat bath temperature. This intriguing theoretical expectation can be confirmed experimentally by using an electric-circuit setup [19], similar to that in Ref. [13]. Our results are applicable to general nonequilibrium processes reaching (non)equilibrium steady states, which implies that the rare-event measurements for time-integrated quantities (to check the fluctuation theorems) should be carefully carried out because the initial memory may survive forever.

This research was supported by the NRF Grant No. 2011-35B-C00014 (J.S.L.) and by Mid-career Researcher Program through NRF Grant No. 2010-0026627 (C.K. and H.P.) funded by the MEST.

[1] D. J. Evans, E. G. D. Cohen, and G. P. Morriss, Phys. Rev. Lett. **71**, 2401 (1993).
[2] G. Gallavotti and E. G. D. Cohen, Phys. Rev. Lett. **74**, 2694 (1995).
[3] C. Jarzynski, Phys. Rev. Lett. **78**, 2690 (1997).
[4] J. Kurchan, J. Phys. A: Math. Gen. **31**, 3719 (1998).
[5] J. L. Lebowitz and H. Spohn, J. Stat. Phys. **95**, 333 (1999).
[6] J. Farago, J. Stat. Phys. **107**, 781 (2002); Physica A **331**, 69 (2004).
[7] R. van Zon and E. G. D. Cohen, Phys. Rev. Lett. **91**, 110601 (2003); Phys. Rev. E **69**, 056121 (2004).
[8] A. Puglisi, L. Rondoni, and A. Vulpiani, J. Stat. Mech.: Theory Exp. (2006) P08010.
[9] R. J. Harris, A. Rákos, and G. M. Schütz, Europhys. Lett. **75**, 227 (2006).
[10] P. Visco, J. Stat. Mech.: Theory Exp. (2006) P06006.
[11] S. Sabhapandit, Europhys. Lett. **96**, 20005 (2011); Phys. Rev. E **85**, 021108 (2012).
[12] General fluctuation relations for heat can be found in J. D. Noh and J.-M. Park, Phys. Rev. Lett. **108**, 240603 (2012).
[13] R. van Zon, S. Ciliberto, and E. G. D. Cohen, Phys. Rev. Lett. **92**, 130601 (2004); S. Ciliberto, S. Joubaud, and A. Petrosyan, J. Stat. Mech.: Theory Exp. (2010) P12003.
[14] H. Park (unpublished).
[15] Farago studied the same model with the $\beta = 1$ and δ-function initial conditions [6].
[16] F. W. Wiegel, *Introduction to Path-Integral Methods in Physics and Polymer Science* (World Scientific, Singapore, 1986).
[17] J. S. Lee, C. Kwon, and H. Park (unpublished).
[18] C. Kwon, J. D. Noh, and H. Park, Phys. Rev. E **83**, 061145 (2011).
[19] J. S. Lee, C. Kwon, and H. Park (unpublished).